Hindawi Publishing Corporation
Journal of Nanomaterials
Volume 2016, Article ID 6729032, 9 pages
http://dx.doi.org/10.1155/2016/6729032

Research Article

XPS Studies of Electrodeposited Grown F-Doped ZnO Rods and Electrical Properties of p-Si/n-FZN Heterojunctions

Saliha Ilican, Mujdat Caglar, Seval Aksoy, and Yasemin Caglar

Science Faculty, Physics Department, Anadolu University, 26470 Eskisehir, Turkey

Correspondence should be addressed to Mujdat Caglar; mcaglar@anadolu.edu.tr

Received 11 April 2016; Revised 20 May 2016; Accepted 23 May 2016

Academic Editor: Mohamed Bououdina

The chemical composition of the electrodeposited undoped and F-doped ZnO (FZN) rods was investigated by X-ray photoelectron spectroscopy (XPS). These results confirmed the existence of F as a doping element into ZnO crystal lattice. The *p-Si/n-ZnO* and *p-Si/n-FZN* heterojunction diodes were fabricated and their electrical properties were investigated. Some parameters belong to these diodes such as ideality factor (n), barrier height (ϕ_B), and series resistance (R_s) which were calculated from the current-voltage (I-V) curves that exhibited rectifying behavior by using thermionic emission theory, Norde's function, and Cheung's method. There is a good agreement between the diode parameters obtained from different methods.

1. Introduction

In recent years, among the transparent oxide semiconductors, zinc oxide (ZnO) based materials have been the focus of many researches. This is because these materials are suitably used in many areas of technology such as field effect transistors [1–3], homojunction or heterojunction diodes [4–6], sensors [7, 8], antireflective coatings [9], and solar cells [10] because of the excellent superior optical properties and electrical performance. Furthermore, large substrates of ZnO are widely available, enabling homoepitaxial growth of ZnO devices, potentially crating a powerful competitor to the nitrides. Moreover, the doped ZnO with various elements such as Al [11], B [12], N [13], In [14], Mn [15], Li [16], Co [17], Sb [18], and Na [19] will increase the film conductivity without substantially influencing the optical transparency.

Until now, fluorine doped ZnO (FZN) films have been studied and produced in many different methods such as hydrothermal synthesis [20], spray pyrolysis [21, 22], aerosol assisted chemical vapor deposition [23] and sol-gel spin coating [24–26], magnetron sputtering [27, 28], pulsed laser deposition [29], and electrodeposition [30]. Among these, electrochemical deposition is a low-cost alternative for the film synthesis, as it does not require complex and expensive equipment and uses easily available raw materials. This simple method provides the possibility of depositing films on substrates with a complex geometry and it can be carried out at low processing temperatures and with low energy consumption. Electrodeposition allows an easy control of the composition, morphology, and thickness of the coatings through the variation of the deposition parameters.

Nam and Kwon [26] prepared FZN films on glass substrate by sol-gel spin coating method and they reported a minimum electrical resistivity for 2.0 at.% F after the first post-heat-treatment (550°C) in air. But after exposing the second annealing (450°C) in a reducing environment (5% H_2 to 95% N_2), they did not observe any significant effect on the electrical resistivity of the FZN films. Tsai et al. [27] prepared FZN films at 150°C on glass substrate by radio frequency magnetron sputtering method. In this work which was aimed at improving the electrical and optical properties of the films, by using thermal annealing under vacuum, it was reported that the lowest resistivity, the highest mobility, the highest carrier concentration, and the highest energy band gap were found to be $1.86 \times 10^{-3}\ \Omega$ cm, 8.9 cm^{2}V^{-1}s^{-1}, 3.78×10^{20} cm^{-3}, and 3.40 eV for the FZN film annealed at 400°C, respectively. Zhang et al. [28] prepared FZN films on flexible substrates by magnetron sputtering at room temperature. In their study,

lowest resistivity of $7.66 \times 10^{-2}\ \Omega$ cm with carrier concentration of $1.31 \times 10^{20}\ \text{cm}^{-3}$ and Hall mobility of $0.62\ \text{cm}^2\text{V}^{-1}\text{s}^{-1}$ were reported. And also average optical transmittance for all doped films was determined to be about 80% in the spectrum range of 300–2000 nm. Cao et al. [29] also reported better results within the scope of electrical property for FZN films deposited by pulsed laser deposition method.

In a previous work of our group, the structural, morphological, and optical properties of electrodeposited FZN rods were firstly reported [30]. In this work, high resolution electron microscopy (SEM) images exhibited the presence of rods and also showed that the diameter and length of these rods increased with doping. Also the maximum density of these rods was obtained at the doping concentration of 15%. Furthermore, the surface propagation deteriorated due to excess F doping and aggregation of the rods as flower structure was observed in many doping levels. XRD results presented that F doping into the ZnO lattice caused a change in preferred orientation of the rods having hexagonal wurtzite structure and deteriorated the crystal structure. Although many researchers have studied the preparation and characterization of FZN, p-n heterojunction diodes applications using FZN has not been studied yet. The difference of this study from the above-mentioned previous works is firstly to make surface chemistry analysis of electrodeposited FZN rods, to fabricate of p-n heterojunction diodes by using these electrodeposited FZN, and to investigate the effect of incorporated fluorine on the electrical performance of the heterojunction diodes. So, this work is the first report on the investigation of electrical properties of *p-Si/n-FZN* diode fabricated by electrodeposition method.

2. Experimental

The undoped and F-doped (1, 5, 10, 15, and 35 at.%) ZnO (1FZN, 5FZN, 10FZN, 15FZN, and 35FZN, resp.) rods were electrochemically deposited on p-Si from aqueous route using chronoamperometry method. A three-electrode system was used for the electrochemical experiments. Experimental details for deposition can be found in a previous work in our group [30]. And then ohmic contacts were made onto surface of the film, patterned with a shadow mask by circular dots of 0.5 mm in diameter. For this contact, the high purity aluminum (Al, 99.999%) with a thickness of 150 nm was thermally evaporated on the film surface. Ohmic behavior of these contacts was confirmed by *I-V* measurements. After these processes, for back ohmic contact, the silver (Ag) paste was applied to back surface of the Si wafer. Any annealing process was not applied to get low resistivity of ohmic contact because of having high eutectic temperature (~830°C) of silver, because such a high temperature can change all the physical properties of samples. The fabricated *p-Si/n-ZnO* and *p-Si/n-XFZN* ($X = 1, 5, 10, 15$, and 35) heterojunction diodes are named D0, D1, D5, D10, D15, and D35, respectively. The schematic structure of these diodes is given in Figure 1 with the SEM image of the 15FZN rods as inset.

For the evaporation of aluminum contacts, thermal evaporation system (Vaksis PVD-HANDY/MT/101T) was used. X-ray photoelectron spectroscopy (XPS) (SPECS) was used to determine fluorine concentration in ZnO and bonding states of related elements using $\text{Al}_{\text{K}\alpha}$ X-rays. The *I-V* characterizations were carried out by using Keithley 4200 SCS and Signatone probe station inside dark box.

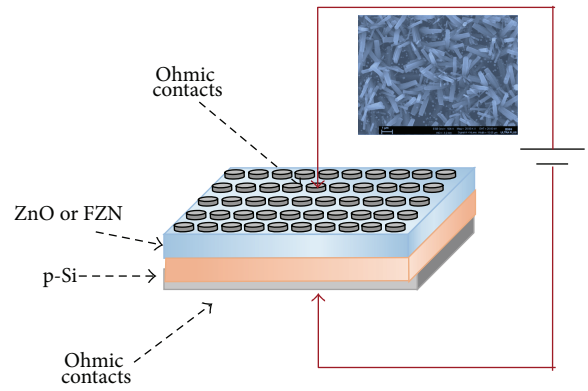

Figure 1: The schematic diagram of the fabricated heterojunction diodes and SEM image of 15FZN inset in figure.

3. Results and Discussion

3.1. XPS Studies of FZN Rods. XPS, which is one of the most important material characterization techniques, has been carried out to both estimate the contained F concentration in the films and determine the chemical states of the film composing elements. In this scope, XPS analyses were carried out for 5FZN, 10FZN, and 15FZN rods. In this analysis, the calibration was made according to C 1s peak at 284.6 eV, but any etching process that is used to remove surface contaminants was not performed. Therefore, the excessive amount of C observed on the survey spectra (Figure 2) is because of not performing any etching procedure. Even so, the peaks belong to F 1s and the expected increase in doping ratio can be seen in Figure 2. The atomic ratio of F/Zn in these samples has been calculated from the XPS survey spectra to be about 0.00417, 0.00825, and 0.01671 for 5FZN, 10FZN, and 15FZN, respectively. These values are approximately ten times lower than the expected nominal compositions because no etching process was applied.

The XPS survey spectra of the nonion bombarded revealed that zinc, oxygen, aluminum, silver, silicon, fluorine, and carbon are present in the FZN rods. The excessive carbon signal corresponds to the contamination of hydrocarbon atoms on the surface. Also aluminum and silicon signals are related to metals contacts on the surface and substrate, respectively. Where silver signal comes from is not known.

The peaks corresponding to F 1s orbital for each doping level are shown in Figure 3. The intensity of F 1s signals increases with increasing doping level and confirms the increase in doping ratio of fluorine as planned before. The observed fluorine 1s signals in this work can be assigned to the formation of Zn-F bonds formed in the ZnO lattice. The peaks located at around 684 eV are close to typical value of binding energy of F 1s peak in fluorine compounds. These

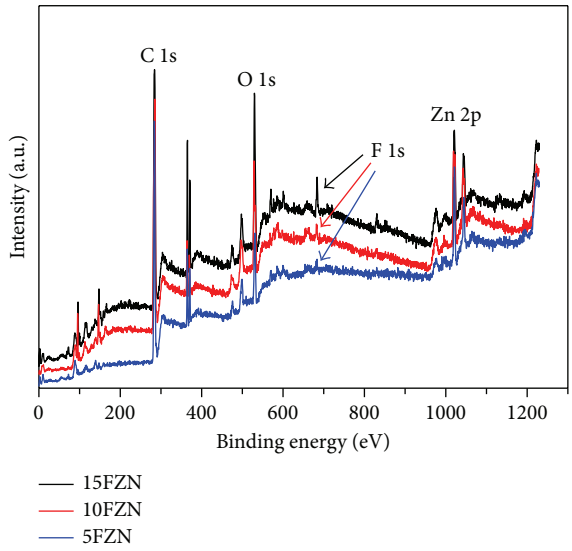

Figure 2: XPS survey spectra of 5FZN, 10FZN, and 15FZN.

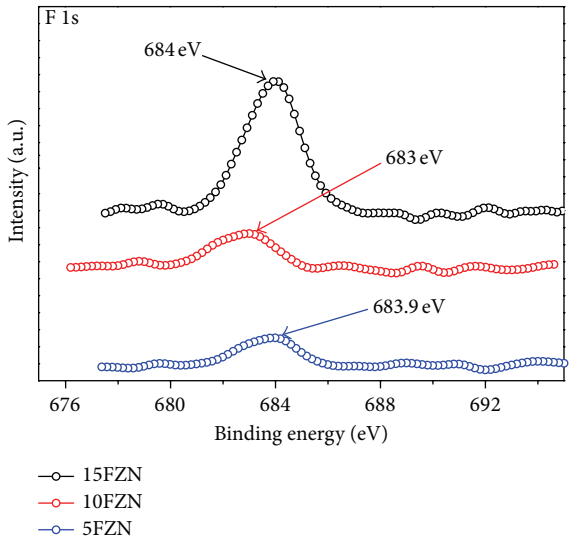

Figure 3: The peaks corresponding to F 1s orbital for each doping level.

signals indicate that F is bonded to the Zn^{+2} and the doping process is performed successfully [31, 32].

The binding states of O 1s spectra belonging to three different rates of FZN are shown in Figure 4. While a single peak having a binding energy at about 530.95 eV is observed for 5FZN rod, 10FZN and 15FZN have exhibited the peaks resolved into three components, which are low binding energy peak, middle binding energy peak, and high binding energy peak. These peaks are centered at about 528.95 eV, 530.99 eV, and 532.45 eV for 10FZN and 529.21 eV, 530.26 eV, and 532.12 eV for 15FZN, respectively. The low and the middle binding energy peaks indicated with O1 and O2 can be attributed to O^{2-} ions at the intrinsic sites and O^{2-} ions in the oxygen deficient regions, respectively [19, 33–35]. The high binding energy component indicated with O3 is also usually attributed to the presence of loosely bound oxygen on the surface of ZnO film such as $-CO_3$, adsorbed H_2O, and adsorbed O_2 [19, 33–35]. Figure 5 gives the typical XPS data of Zn $2p_{3/2}$ for three samples. In this figure the effect of fluorine in the ZnO lattice because Zn $2p_{3/2}$ peaks are resolved into two components which are located at low and high binding energy values can be seen. The observed peaks at high binding energy confirm the formation of zinc-fluorine bond, because, in the previous reported studies related to F-doped ZnO, the signal centered at 1022.52 eV was attributed to Zn-F bonds [31]. So, the signals centered at 1022.9 eV and 1022.48 eV can be attributed to the Zn-F bond that means the fluorine substitution of the oxygen atom. Also the signals observed at about 1020 eV could be attributable to the Zn-O bond in the ZnO.

3.2. I-V Characteristics of p-Si/n-ZnO and p-Si/n-FZN Heterojunctions. Figure 6 shows the *I-V* characteristics of *p-Si/n-ZnO* and *p-Si/n-FZN* diodes. It is evident from this figure that the fabricated junction shows rectifying behavior. It can be seen that the rectification ratio is between 10^3 and 10^4 and this ratio increases at first with fluorine content but the highest ratio is observed in D35. A thermionic emission model that is given in the following relation can describe the nonlinear *I-V* characteristic of a heterojunction [36]:

$$I = I_o\left[\left(\exp\left(\frac{qV}{nkT}\right)\right) - 1\right], \quad (1)$$

where I_o, q, n, k, T, and V are the saturation current, the electronic charge, the ideality factor, the Boltzmann constant and the temperature (in kelvin), and the applied voltage, respectively. n values were determined from the slope of the linear regions of the forward bias *I-V* curves. The calculated n values of the fabricated heterojunction diodes are given in Table 1. In all diodes, nonideal behavior can be seen because ideality factor values are greater than 1, meaning the presence of inhomogeneity in barrier height and presence of interface states.

The barrier height (ϕ_B) of the diode is calculated using the following equation [36]:

$$I_o = AA^*T^2\exp\left(\frac{-q\phi_B}{kT}\right), \quad (2)$$

where A is the diode contact area and A^* is the Richardson constant. The calculated ϕ_B values are given in Table 1. These values are close to the difference of the work functions of Si (4.97 eV) and ZnO (4.25 eV), that is, 0.72 eV. The barrier height of these diodes is in agreement with the heterojunction diodes (undoped or doped ZnO with different elements used as n-ZnO) in the literature [6, 17, 37–40]. There is only one study on the ideality factor of electrodeposited ZnO based heterojunction diode in available literature [17] and the ideality factor value which was reported for *n-ZnO/p-Si* heterojunction (5.48) is higher than the values of present work, although deposition parameters of both the same methods are not same.

Table 1: The diode parameters of the fabricated heterojunction diodes.

Diode	*I-V*		Cheung-Cheung				Norde	
			Cheung	*H* function				
	n	ϕ_B (eV)	R_s (kΩ)	n	R_s (kΩ)	ϕ_B (eV)	R_s (kΩ)	ϕ_B (eV)
D0	3.87	0.74	76.21	3.44	290.00	0.80	19.30	0.82
D1	4.05	0.73	105.98	3.85	300.07	0.70	119.00	0.77
D5	4.31	0.68	107.97	4.49	240.82	0.57	66.30	0.71
D10	3.06	0.73	81.44	3.86	149.25	0.69	96.00	0.77
D15	3.98	0.68	52.64	4.10	88.95	0.65	1.94	0.71
D35	3.96	0.72	55.81	5.50	325.67	0.46	54.10	0.73

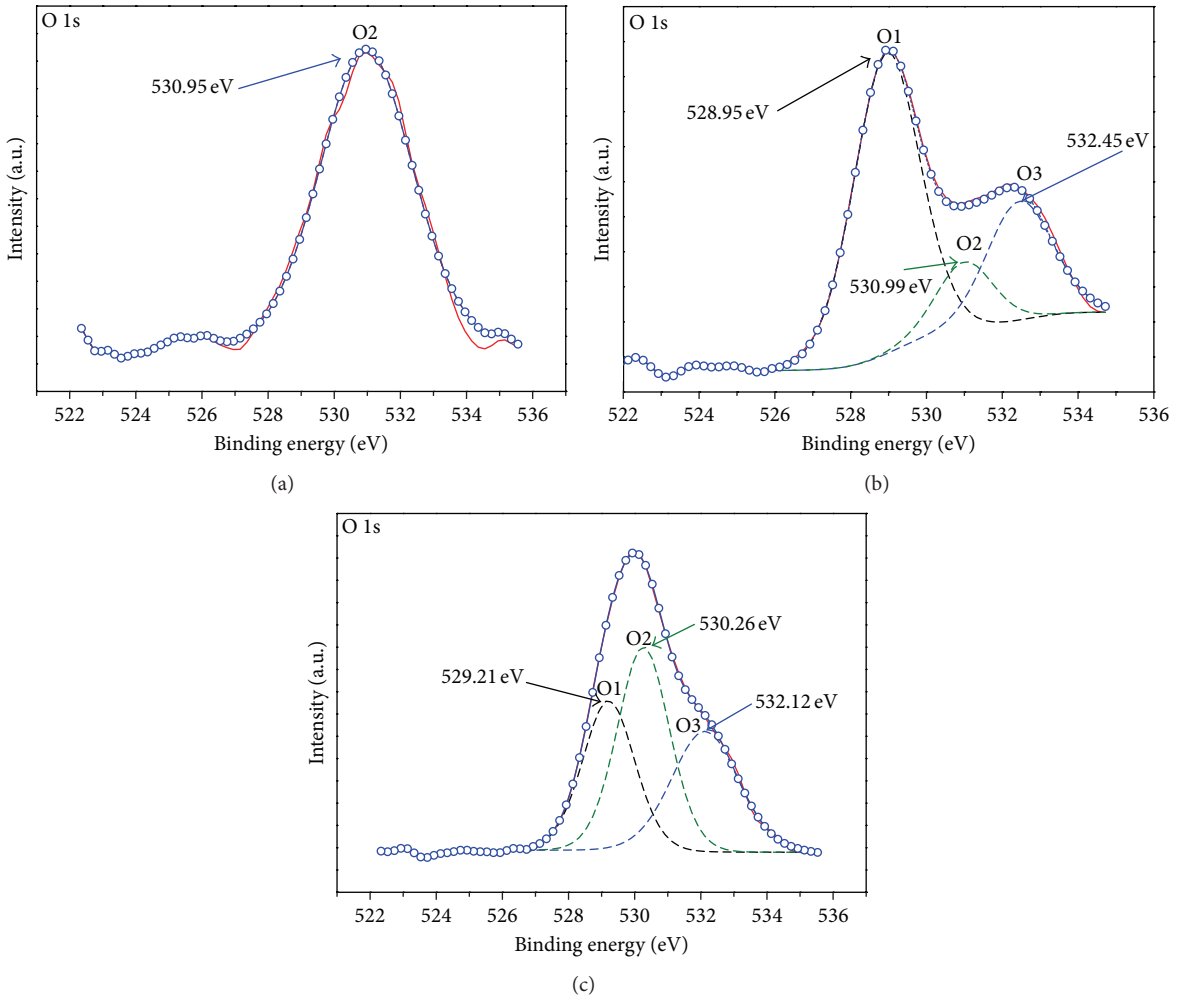

Figure 4: XPS spectra (open circles) and simulated lines of O 1s in the ZnO: (a) 5FZN, (b) 10FZN, and (c) 15FZN.

Furthermore, to determine the ϕ_B value, an alternative method was defined by Norde using the following function [41]:

$$F(V) = \frac{V}{\gamma} - \left(\frac{kT}{q}\right) \ln\left(\frac{I(V)}{AA^*T^2}\right), \tag{3}$$

where γ is the first integer (dimensionless) greater than n. The ϕ_B values were calculated from the minimum of the $F(V)$-V curve. Figure 7 shows $F(V)$ versus V plot of the fabricated heterojunction diodes. The ϕ_B values were determined from following relation:

$$\phi_B = F(V_0) + \frac{V_0}{\gamma} - \frac{kT}{p}, \tag{4}$$

where $F(V_0)$ is the minimum point of $F(V)$ and V_0 is the corresponding voltage. The value of series resistance (R_s) was calculated using the formula

$$R_s = \frac{kT(\gamma - n)}{qI}. \tag{5}$$

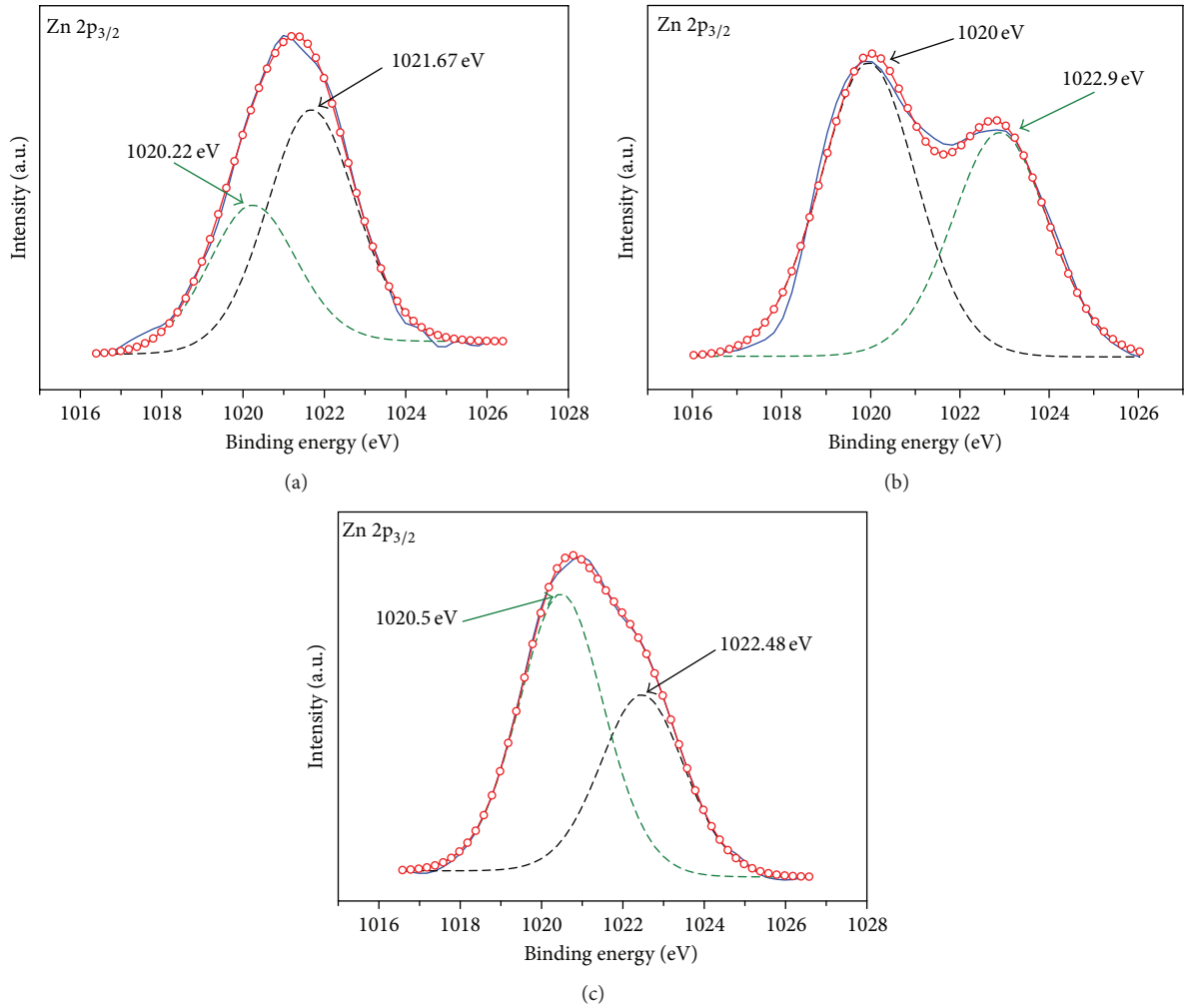

FIGURE 5: XPS spectra (open circles) and simulated lines of Zn $2p_{3/2}$ in the ZnO: (a) 5FZN, (b) 10FZN, and (c) 15FZN.

The ϕ_B and R_s values of the fabricated heterojunction diodes were given in Table 1.

The n and R_s values were also determined using Cheung's method. According to this method, the forward bias I-V characteristics of a device having series resistance are given as

$$I = I_o \exp\left(\frac{q(V - IR_s)}{nkT}\right). \quad (6)$$

To determine the n and R_s values, the following equation was also used:

$$\frac{dV}{d(\ln I)} = IR_s + \frac{nkT}{q}. \quad (7)$$

The forward bias $dV/d(\ln I)$-I plots of the fabricated heterojunction diodes are given in Figure 8. The slope of these plots gives the R_s values and intercept gives the n value of these diodes. These calculated values for fabricated heterojunction diodes were given in Table 1. The observed difference between the n values that were obtained from the forward bias semilog I-V plots and from the $dV/d(\ln I)$-I plots may be due to presence of series resistance and undesirable interface states [42].

The ϕ_B and R_s values were also determined by using $H(I)$ function [43]:

$$H(I) = n\phi_B + IR_s, \quad (8)$$

where

$$H(I) = V - \frac{nkT}{q}\ln\left(\frac{I}{AA^*T^2}\right). \quad (9)$$

A plot of $H(I)$ versus I is linear, the slope of this plot gives R_s value, and intercept gives the ϕ_B value. These values given in Table 1 were calculated from $H(I)$ versus I plots (Figure 8). As observed, there is a small difference between R_s values determined from Cheung's and Norde's method. This difference may be due to the applicability of both methods in different voltages regions.

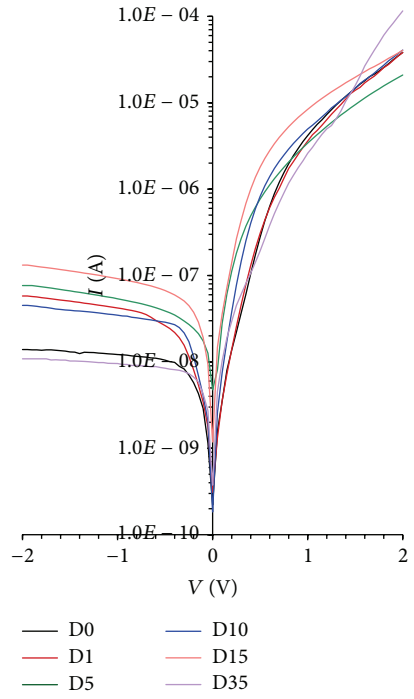

Figure 6: Semilog I-V characteristics of the fabricated heterojunction diodes under dark.

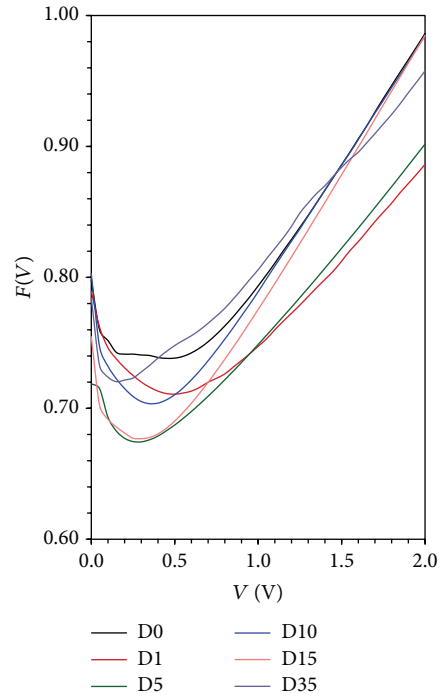

Figure 7: $F(V)$-V plots of the fabricated heterojunction diodes.

In general, the R_s values are tendency of decreasing with F content. As seen in Table 1, some of these R_s values are larger than expected (≥100 kΩ). These high values may be caused by the quality of back ohmic contact, that is; this result refers to the effect of interface states between p-Si and silver. Therefore, in the literature, it is possible to find many reports related to R_s values having low resistivity by applying annealing process [44, 45]. Furthermore, some experimental studies in literature have also reported that R_s value could be either increased or decreased by using organic/inorganic layer on inorganic Si semiconductor [15, 46, 47].

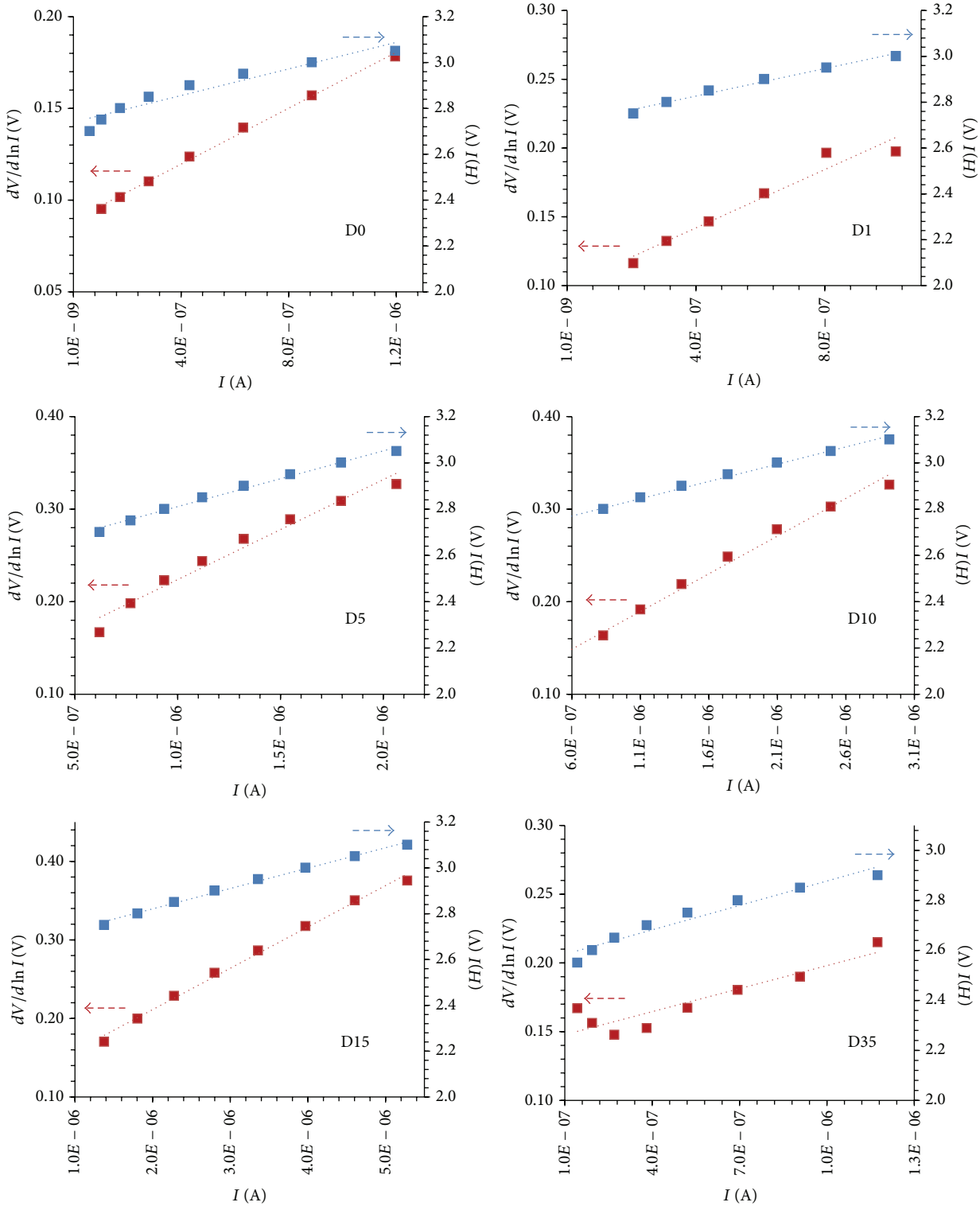

Figure 8: The forward bias $dV/d(\ln I)$-I and $H(I)$-I plots of the fabricated heterojunction diodes.

4. Conclusion

ZnO and FZN rods were deposited by electrochemical deposition method. To investigate fluorine concentration into ZnO, XPS analysis was used and the existence of fluorine and its atomic ratio were determined as 0.00417, 0.00825, and 0.01671 for 5FZN, 10FZN, and 15FZN, respectively. Electrical properties of p-n heterojunctions based on electrodeposited ZnO and FZN were characterized using I-V measurements and some diode parameters were determined. The obtained

parameters using different methods were compared and discussed depending on the fluorine content.

Competing Interests

The authors declare that they have no competing interests.

Acknowledgments

This work was supported by Anadolu University Commission of Scientific Research Project under Grant nos. 1207F118 and 1402F055.

References

[1] T. S. Lin and C. T. Lee, "Homostructured ZnO-based metal-oxide-semiconductor field-effect transistors deposited at low temperature by vapor cooling condensation system," *Applied Surface Science*, vol. 354, pp. 71–73, 2015.

[2] S. Ruzgar and S. Aksoy, "Electrical performance of ZnO thin film transistors having different active layer thickness," *Journal of Materials and Electronic Devices*, vol. 1, pp. 38–41, 2015.

[3] S. Ruzgar, A. E. Ozkan, M. Caglar et al., "Effect of the deposition temperature on the device performance of the nanostructured ZnO thin film transistor by sol gel method," *Journal of Nanoelectronics and Optoelectronics*, vol. 9, no. 5, pp. 689–693, 2014.

[4] S. Yilmaz, I. Polat, Ş. Altindal, and E. Bacaksiz, "Structural and electrical characterization of rectifying behavior in n-type/intrinsic ZnO-based homojunctions," *Materials Science and Engineering B: Solid-State Materials for Advanced Technology*, vol. 177, no. 8, pp. 588–593, 2012.

[5] S. A. Mansour and F. Yakuphanoglu, "Electrical-optical properties of nanofiber ZnO film grown by sol gel method and fabrication of ZnO/p-Si heterojunction," *Solid State Sciences*, vol. 14, no. 1, pp. 121–126, 2012.

[6] A. Arslan, E. Hür, S. Ilican, Y. Caglar, and M. Caglar, "Controlled growth of c-axis oriented ZnO nanorod array films by electrodeposition method and characterization," *Spectrochimica Acta—Part A: Molecular and Biomolecular Spectroscopy*, vol. 128, pp. 716–723, 2014.

[7] T. Sin Tee, T. Chun Hui, C. Wu Yi et al., "Microwave-assisted hydrolysis preparation of highly crystalline ZnO nanorod array for room temperature photoluminescence-based CO gas sensor," *Sensors and Actuators B: Chemical*, vol. 227, pp. 304–312, 2016.

[8] Y. Şahin, S. Öztürk, N. Kılınç, A. Kösemen, M. Erkovan, and Z. Z. Öztürk, "Electrical conduction and NO_2 gas sensing properties of ZnO nanorods," *Applied Surface Science*, vol. 303, pp. 90–96, 2014.

[9] T. Minemoto, T. Mizuta, H. Takakura, and Y. Hamakawa, "Antireflective coating fabricated by chemical deposition of ZnO for spherical Si solar cells," *Solar Energy Materials and Solar Cells*, vol. 91, no. 2-3, pp. 191–194, 2007.

[10] B. Kilic, T. Günes, I. Besirli, M. Sezginer, and S. Tuzemen, "Construction of 3-dimensional ZnO-nanoflower structures for high quantum and photocurrent efficiency in dye sensitized solar cell," *Applied Surface Science*, vol. 318, pp. 32–36, 2014.

[11] L. Liu, L. Wang, X. Qin, L. Cui, and G. Shao, "Effects of intermittent atomization on the properties of Al-doped ZnO thin films deposited by aerosol-assisted chemical vapor deposition," *Thin Solid Films*, vol. 605, pp. 163–168, 2016.

[12] F. Yakuphanoglu, Y. Caglar, M. Caglar, and S. Ilican, "Electrical characterization of the diodes-based nanostructure ZnO:B," *EPJ Applied Physics*, vol. 58, no. 3, Article ID 30101, 2012.

[13] S. Aksoy and S. Ruzgar, "Effect of N doped on optical properties of ZnO film deposited by sol gel," *Journal of Materials and Electronic Devices*, vol. 1, no. 1, pp. 33–37, 2015.

[14] A. Singh, S. Chaudhary, and D. Pandya, "High conductivity indium doped ZnO films by metal target reactive co-sputtering," *Acta Materialia*, vol. 111, pp. 1–9, 2016.

[15] I. Taşçıoğlu, W. A. Farooq, R. Turan, S. Altındal, and F. Yakuphanoglu, "Charge transport mechanisms and density of interface traps in MnZnO/p-Si diodes," *Journal of Alloys and Compounds*, vol. 590, pp. 157–161, 2014.

[16] V. Bornand and A. Mezy, "Morphological and ferroelectric studies of Li-doped ZnO thin films," *Materials Letters*, vol. 107, pp. 357–360, 2013.

[17] Y. Caglar, A. Arslan, S. Ilican, E. Hür, S. Aksoy, and M. Caglar, "Preparation and characterization of electrodeposited ZnO and ZnO:Co nanorod films for heterojunction diode applications," *Journal of Alloys and Compounds*, vol. 574, pp. 104–111, 2013.

[18] J. K. Liang, H. L. Su, C. L. Kuo et al., "Structural, optical and electrical properties of electrodeposited Sb-doped ZnO nanorod arrays," *Electrochimica Acta*, vol. 125, pp. 124–132, 2014.

[19] S. Ilican, "Effect of Na doping on the microstructures and optical properties of ZnO nanorods," *Journal of Alloys and Compounds*, vol. 553, pp. 225–232, 2013.

[20] M. W. Kadi, D. McKinney, R. M. Mohamed, I. A. Mkhalid, and W. Sigmund, "Fluorine doped zinc oxide nanowires: enhanced photocatalysts degrade malachite green dye under visible light conditions," *Ceramics International*, vol. 42, no. 4, pp. 4672–4678, 2016.

[21] E. Şennik, S. Kerli, Ü. Alver, and Z. Z. Öztürk, "Effect of fluorine doping on the NO_2-sensing properties of ZnO thin films," *Sensors and Actuators, B: Chemical*, vol. 216, pp. 49–56, 2015.

[22] F. Yakuphanoglu, Y. Caglar, S. Ilican, and M. Caglar, "The effects of fluorine on the structural, surface morphology and optical properties of ZnO thin films," *Physica B: Condensed Matter*, vol. 394, no. 1, pp. 86–92, 2007.

[23] M. Anusha and D. Arivuoli, "High intense violet luminescence in fluorine doped zinc oxide (FZO) thin films deposited by aerosol assisted CVD," *Journal of Alloys and Compounds*, vol. 580, pp. 131–136, 2013.

[24] S. Ilican, Y. Caglar, M. Caglar, and F. Yakuphanoglu, "Structural, optical and electrical properties of F-doped ZnO nanorod semiconductor thin films deposited by sol-gel process," *Applied Surface Science*, vol. 255, no. 5, pp. 2353–2359, 2008.

[25] J. Podporska-Carroll, A. Myles, B. Quilty et al., "Antibacterial properties of F-doped ZnO visible light photocatalyst," *Journal of Hazardous Materials*, 2015.

[26] G. M. Nam and M. S. Kwon, "F-doped ZnO by sol-gel spin-coating as a transparent conducting thin film," *Electronic Materials Letters*, vol. 7, no. 2, pp. 127–131, 2011.

[27] Y.-Z. Tsai, N.-F. Wang, and C.-L. Tsai, "Fluorine-doped ZnO transparent conducting thin films prepared by radio frequency magnetron sputtering," *Thin Solid Films*, vol. 518, no. 17, pp. 4955–4959, 2010.

[28] X. Zhang, L. Zhu, H. Xu, L. Chen, Y. Guo, and Z. Ye, "Highly transparent conductive F-doped ZnO films in wide range of visible and near infrared wavelength deposited on polycarbonate substrates," *Journal of Alloys and Compounds*, vol. 614, pp. 71–74, 2014.

[29] L. Cao, L. P. Zhu, W. F. Chen, and Z. Z. Ye, "Preparation and thermal stability of F-doped ZnO transparent conducting thin films," *Optical Materials*, vol. 35, no. 6, pp. 1293–1296, 2013.

[30] P. Bilgic Ozden, A. Arslan, B. Arpapay et al., "Structural and optical properties of electrochemically grown fluorine doped zinc oxide rods," *Journal of Nanoelectronics and Optoelectronics*, vol. 9, no. 5, pp. 590–595(6), 2014.

[31] G. H. Kim, D. H. Hwang, and S. I. Woo, "Effect of fluorine addition on boron doped ZnO transparent electrode by room temperature spray method and thermal treatment," *Materials Chemistry and Physics*, vol. 131, no. 1-2, pp. 77–83, 2011.

[32] S. W. Gaarenstroom and N. Winograd, "Initial and final state effects in the ESCA spectra of cadmium and silver oxides," *The Journal of Chemical Physics*, vol. 67, no. 8, pp. 3500–3506, 1977.

[33] Y. Caglar, "Sol-gel derived nanostructure undoped and cobalt doped ZnO: structural, optical and electrical studies," *Journal of Alloys and Compounds*, vol. 560, pp. 181–188, 2013.

[34] M. Caglar and F. Yakuphanoglu, "Structural and optical properties of copper doped ZnO films derived by sol-gel," *Applied Surface Science*, vol. 258, no. 7, pp. 3039–3044, 2012.

[35] S. Aksoy, Y. Caglar, S. Ilican, and M. Caglar, "Sol-gel derived Li-Mg co-doped ZnO films: preparation and characterization via XRD, XPS, FESEM," *Journal of Alloys and Compounds*, vol. 512, no. 1, pp. 171–178, 2012.

[36] S. M. Sze and K. N. Kwok, *Physics of Semiconductor Devices*, Wiley, New York, NY, USA, 2007.

[37] F. Yakuphanoglu, Y. Caglar, M. Caglar, and S. Ilican, "ZnO/p-Si heterojunction photodiode by solgel deposition of nanostructure n-ZnO film on p-Si substrate," *Materials Science in Semiconductor Processing*, vol. 13, no. 3, pp. 137–140, 2010.

[38] M. Cavas, A. A. M. Farag, Z. A. Alahmed, and F. Yakuphanoglu, "Photosensors based on Ni-doped ZnO/p-Si junction prepared by sol-gel method," *Journal of Electroceramics*, vol. 31, no. 3-4, pp. 298–308, 2013.

[39] F. Yakuphanoglu, "Controlling of electrical and interface state density properties of ZnO:Co/p-silicon diode structures by compositional fraction of cobalt dopant," *Microelectronics Reliability*, vol. 51, no. 12, pp. 2195–2199, 2011.

[40] C.-C. Wu and C.-F. Yang, "Effect of annealing temperature on the characteristics of the modified spray deposited Li-doped NiO films and their applications in transparent heterojunction diode," *Solar Energy Materials and Solar Cells*, vol. 132, pp. 492–498, 2015.

[41] H. Norde, "A modified forward I-V plot for Schottky diodes with high series resistance," *Journal of Applied Physics*, vol. 50, no. 7, pp. 5052–5053, 1979.

[42] F. Yakuphanoglu, M. Shah, and W. A. Farooq, "Electrical and interfacial properties of p-Si/P3HT organic-on-inorganic junction barrier," *Acta Physica Polonica A*, vol. 120, no. 3, pp. 558–562, 2011.

[43] S. K. Cheung and N. W. Cheung, "Extraction of Schottky diode parameters from forward current-voltage characteristics," *Applied Physics Letters*, vol. 49, no. 2, pp. 85–89, 1986.

[44] M. Gokcen, T. Tunc, S. Altindal, and I. Uslu, "Electrical and photocurrent characteristics of Au/PVA (Co-doped)/n-Si photoconductive diodes," *Materials Science and Engineering B*, vol. 177, no. 5, pp. 416–420, 2012.

[45] Ç. Bilkan, S. Zeyrek, S. E. San, and Ş. Altindal, "A compare of electrical characteristics in Al/p-Si (MS) and Al/$C_{20}H_{12}$/p-Si (MPS) type diodes using current-voltage (*I-V*) and capacitance-voltage (*C-V*) measurements," *Materials Science in Semiconductor Processing*, vol. 32, pp. 137–144, 2015.

[46] A. A. Hendi and F. Yakuphanoglu, "Graphene doped TiO_2/p-silicon heterojunction photodiode," *Journal of Alloys and Compounds*, vol. 665, pp. 418–427, 2016.

[47] P. Giri and P. Chakrabarti, "Effect of Mg doping in ZnO buffer layer on ZnO thin film devices for electronic applications," *Superlattices and Microstructures*, vol. 93, pp. 248–260, 2016.